Journal of Alloys and Compounds 509 (2011) 7692–7696

Contents lists available at ScienceDirect

Journal of Alloys and Compounds

journal homepage: www.elsevier.com/locate/jallcom

Microstructures and mechanical properties of the *in situ* TiB–Ti metal–matrix composites synthesized by spark plasma sintering process

Xiangbo Shen, Zhaohui Zhang*, Sai Wei, Fuchi Wang, Shukui Lee

School of Materials Science and Engineering, Beijing Institute of Technology, Beijing 100081, China

ARTICLE INFO

Article history:
Received 6 April 2011
Received in revised form 5 May 2011
Accepted 5 May 2011
Available online 12 May 2011

Keywords:
TiB–Ti composites
Microstructure
Mechanical properties
Spark plasma sintering

ABSTRACT

In situ synthesized TiB reinforced titanium matrix composites have been synthesized by spark plasma sintering (SPS) process at 950–1250 °C, using mixtures of 15 wt% TiB_2 and 85 wt% Ti powders. The effects of the sintering temperature on densification behavior and mechanical properties of the TiB–Ti composites were investigated. The results indicated that with rising sintering temperatures, relative densities of the composites increase obviously, while the *in situ* TiB whiskers grow rapidly. As a result, bending strength of the TiB–Ti composites increases slowly at the combined actions of the factors referred above. Fracture toughness of the composites is improved remarkably due to the large volume fraction of Ti matrix, the crack deflection, pull-out and the micro-fracture of the needle-shaped TiB grains. The results also suggested that TiB–Ti composite sintered at 1250 °C by SPS process exhibits the highest relative density of 99.6% along with bending strength of 1161 MPa and fracture toughness of 13.5 MPa $m^{1/2}$.

1. Introduction

Titanium alloys are widely used in aerospace, chemical, power generation and biomedical industries due to their low density and excellent mechanical strength at ambient temperature [1,2]. However, conventional Ti alloys exhibit inferior wear resistance and suffer considerable loss in mechanical strength at high temperatures. Such drawbacks limit their full potential structural applications in many industrial sectors. *In situ* ceramic particles or whiskers reinforced titanium matrix composites (TMCs) offer a combination of good mechanical properties and high temperature durability such as high specific modulus, excellent high temperature strength and good heat resistance [3–5], due to the thermodynamically stabilization and good mechanical properties of the reinforcements. In the past decades, SiC, TiC, Al_2O_3, and TiB have been used to produce TMCs by self-propagation high-temperature synthesis (SHS) [6,7], mechanical alloying (MA) [8,9], powder metallurgy (PM) [10–12], combustion synthesis [13], rapid solidification processing (RSP) [14,15], vacuum arc remelting (VAR) [16], etc. Among these reinforcements, TiB is outstanding due to its excellent thermodynamically stability and strong interfacial bonding with Ti matrix, as well as the similar thermal expansion coefficient to Ti matrix.

Spark plasma sintering (SPS) is a newly developed consolidation process that enables the composite powder to be fully densified at a comparatively low temperature and in very short time [17–21]. SPS method consists of three main mechanisms of action: (a) the application of uniaxial pressure; (b) the application of pulsed voltage and (c) the resistance heating of graphite dies and sample. Thus, the spark discharge, resistance heating, plastic deformation and boundary cleaning effects all contribute to densification of the powders [22–28]. Therefore, rapid heating is available and the bulk compact with fine grain microstructure can be obtained. The SPS process has been developed for fabricating metals, ceramics, composites, intermetallic compounds, functionally graded materials (FGM) and nanocrystalline materials, which are difficult in sintering by common methods [27,28]. In this study, *in situ* synthesized TiB reinforced titanium matrix composites were fabricated by SPS method, using mixtures of 15 wt% TiB_2 and 85 wt% Ti powder. The microstructures and mechanical properties of the composites sintered at different temperatures were investigated.

2. Experimental procedures

2.1. Starting powders

Commercially available Ti powders (99.8% pure, Mengtai Powder Business Department, Beijing, China) and TiB_2 powders (99.6% pure, Ningxia Machinery Research Institute, Ningxia, China) were used as raw materials. The average particle size of Ti and TiB_2 powders is about 30 μm and 4.5 μm, respectively. TiB was *in situ* synthesized by chemical reaction of Ti with TiB_2 during the SPS process. Mixtures of the composite was prepared by milling 15 wt% TiB_2 and 85 wt% Ti powders in a planetary mill for 2 h at milling rotation speed of 300 rpm, using ethanol and

* Corresponding author. Tel.: +86 10 68912709; fax: +86 10 68913938.
E-mail address: zhang@bit.edu.cn (Z. Zhang).

0925-8388/$ – see front matter © 2011 Elsevier B.V. All rights reserved.
doi:10.1016/j.jallcom.2011.05.017

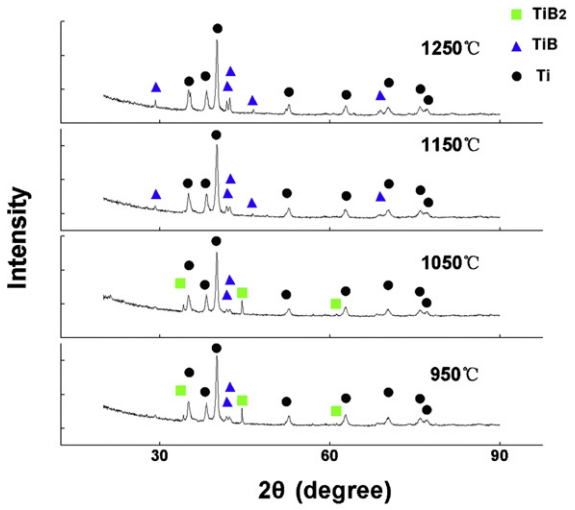

Fig. 1. XRD spectra of the TiB–Ti composites sintered at different temperatures.

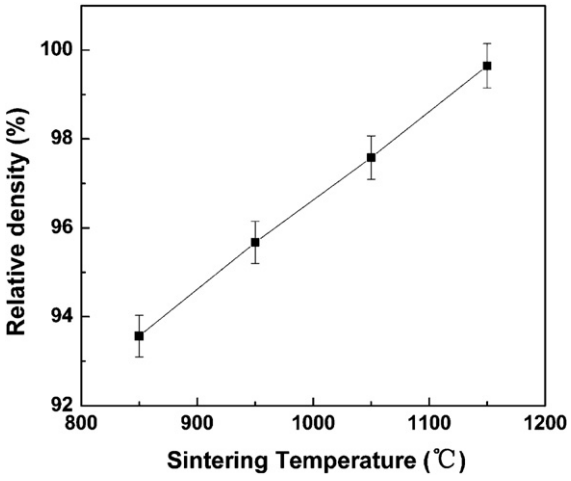

Fig. 2. Influence of sintering temperature on relative density.

agate balls as a milling medium. The weight ratio of balls to powder was fixed to 5:1. The resultant slurry was dried in vacuum evaporator.

2.2. Sintering parameters

DR.SINTER type SPS-3.20 equipment (Sojitz Machinery Corporation, Tokyo, Japan) with pulse duration of 3.3 ms and a current on–off ratio of 12:2 was used in this procedure. The mixtures were sintered in a 0.5 Pa vacuum chamber, using a cylindrical graphite die (Sanye Carbon Group, Beijing, China). The external diameter, internal diameter and height of the die are 90 mm, 40 mm and 80 mm, respectively. A graphite felt was used as thermal insulation. The temperature was examined by the infrared thermometer. The specimen was sintered at temperatures of 950 °C, 1050 °C, 1150 °C, and 1250 °C, with a heating rate of 100 °C/min and holding time of 5 min. Applied initial and holding compressive pressure level was 1 MPa and 50 MPa, respectively.

2.3. Characterization tests

The phase identification was evaluated by X-ray diffraction (XRD) analysis (X' Pert PRO MPD, PANalytical B.V., Netherlands) using Cu K_α radiation. The polished specimens were etched with a solution of 5 ml HF, 10 ml HNO_3 and 85 ml H_2O. Microstructure investigation of the as-sintered composites was carried out by scanning electron microscope (SEM, Hitachi S-4800N, Hitachi, Japan). Vickers hardness of the specimen was tested by the LM700AT micro hardness tester provided by LECO Corporation. Bending strength (σ_b) was evaluated by three-points bending method using an Instron instrument, the dimension of the specimen was 3 mm × 4 mm × 22 mm with a span of 15 mm. The tensile edges were beveled and the tensile surfaces were polished with 1 μm diamond paste. Fracture toughness (K_{IC}) was evaluated by a single-edge notched beam (SENB) method on 2 mm × 4 mm × 15 mm specimens, with a notch of 0.2 mm width and 2 mm depth. At least six specimens were tested for each experimental condition.

3. Results and discussion

3.1. Reaction products

The chemical reaction between Ti and TiB_2 can proceed as follows:

$$Ti + TiB_2 = 2TiB \quad (1)$$

As mentioned above, TiB phase is thermodynamically more stable than TiB_2 phase when excess moles of titanium exist. Therefore, TiB_2 phase is transformed into TiB phase during the fabrication process.

Fig. 1 shows the X-ray diffraction patterns of the composites sintered at different temperatures. Clearly, the phases of the specimens change with increase of the sintering temperatures, as observed from the diffraction peaks of Ti, TiB, and TiB_2 indexed in the spectra. The diffraction peaks of Ti and TiB are present in all these spectra for the composites. No diffraction peak of TiB_2 is observed in the XRD spectra for the composite sintered at 1150 °C, indicating that the chemical reaction shown in Eq. (1) were completed at this sintering temperature and the TiB–Ti composite sintered above1150 °C by SPS process consist of Ti and TiB phases. For the composites sintered at 1250 °C, the intensity of the diffraction peaks of Ti has no obvious change, but that for TiB increase obviously. Since the compositions of the materials are same, the results referred above suggest that the *in situ* TiB grains have grown up at this sintering temperature.

The relative volume fractions of the composition phases can be computed from the integrated intensities of the selected peaks in the X-ray diffraction pattern by the direct comparison method [29,30]. The results indicate that the volume fraction of TiB in the composite sintered at 1250 °C was about 26%, which is corresponding to the theoretical ingredient of the TiB–Ti composite synthesized from the mixtures of 15 wt% TiB_2 and 85 wt% Ti powders.

3.2. Relative density

Fig. 2 presents the curve of sintering temperature versus relative density of the sintered TiB–Ti composites. The plot shows a nearly linear increase of the relative density with sintering temperature, revealing that the sintering temperature has a remarkable influence on the relative density of the sintered specimens. However, increasing rate of the relative density is small. With sintering temperature rising from 950 °C to 1250 °C, the relative density of the bulk compact increases from 93.6% to 99.6%. Nearly fully dense TiB–Ti composite was obtained by SPS at sintering temperature of 1250 °C.

3.3. Microstructure characteristics

TiB has a B27 crystal structure characterized by zig-zag chains of boron atoms parallel to the [0 1 0] direction, which each B atom lying at the center of a trigonal prism of six Ti atoms. Then TiB should exhibit much faster growth along [0 1 0] direction and develop a needle-shaped or rod-like morphology [30,31]. Fig. 3 presents the scanning electron micrographs of a polished and etched surface of the TiB–Ti composites synthesized by SPS process at different sintering temperatures. The images show a relatively homogeneous distribution of reinforcements. The *in situ* synthesized TiB exhibit needle and rod shape with a high aspect ratio and is uniformly distributed in the Ti matrix. With increasing sintering temperature, more and more TiB whiskers was synthesized through the chemical reaction shown in Eq. (1), then the resulting TiB grew and con-

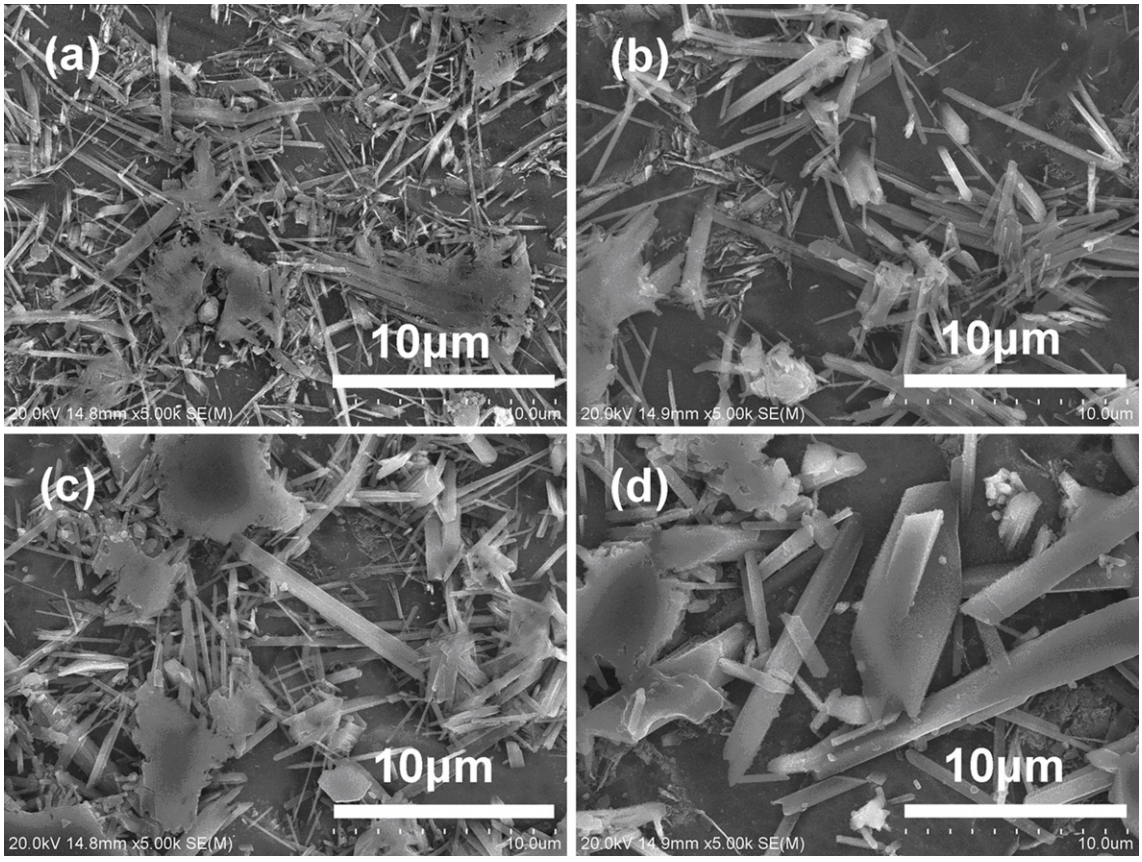

Fig. 3. SEM images of the TiB–Ti composites sintered at temperature: (a) 950 °C, (b) 1050 °C, (c) 1150 °C and (d) 1250 °C.

nected rapidly, making the needle-shaped or rod-like TiB whiskers coarsen and agglomerate obviously. Fig. 3 also indicates that most of the *in situ* synthesized TiB form along Ti grain boundaries and the final size of TiB reinforcements are determined by sintering temperature. Some TiB needles grow into inner of phases from boundaries, which are smaller in size and less in amount, while others grow along the phase boundaries. The diameter of *in situ* TiB is 0.2 μm when sintered at 950 °C and 2 μm when sintered at 1250 °C.

Fig. 4 exhibits the fracture surfaces of the TiB–Ti composites sintered at different temperatures. Large pores can be observed on fracture surface of the composites sintered at 950 °C and 1050 °C, and the porosity of the composites decreases with increasing sintering temperatures. Especially, some unreacted TiB_2 particles are detected on the fracture surface of the composites sintered at 950 °C, indicating that the chemical reaction between Ti and TiB_2 was not completed at this sintering temperature during SPS process. Few pores can be detected on the fracture surface of the composites sintered at 1250 °C, suggesting that the TiB–Ti composite sintered at this temperature by SPS process is nearly fully dense.

Fig. 5 presents the typical fracture surface of the TiB–Ti composite sintered at 1250 °C at high magnification. Hybrid-fracture characteristic appear in the fracture. Pull-out and cleavage fracture take place in the grains of TiB, and the quasi-cleavage fracture appears in the Ti matrix. The special fracture behavior contributes to improve the mechanical properties of the TiB–Ti composites.

3.4. Mechanical properties

Fig. 6 shows the influence of the sintering temperature on micro-hardness of the *in situ* synthesized TiB–Ti composites. Obviously, the micro-hardness distributes in 2 regions: one region has the higher hardness, from 4.4 GPa to 6.6 GPa, with ranging the sintering temperature from 950 °C to 1250 °C. While the other has the lower hardness, from 4.1 GPa to 4.7 GPa. The distribution of the micro-hardness indicates that microstructures of the composites at least have 2 phases with different micro-hardness. The same results can be obtained by the XRD analysis on the TiB–Ti composites sintered at different temperatures as shown in Fig. 1. Fig. 7 exhibits SEM images of the TiB–Ti composite sintered at 1250 °C at low magnification, clearly indicating the composite consist of two phases with different morphology, the needle-shaped TiB whiskers and Ti matrix.

The Vickers hardness of the composites was examined by the micro-hardness tester, and the size of the indentation is about 10 μm. However, the diameter of the TiB grains in the TiB–Ti composites synthesized by SPS technique is much less than the indentation size. Therefore, the indentation areas should include both the TiB grains and Ti matrix, and then the Ti matrix bears part of the load. As a result, the tested micro-hardness of the TiB phase in the TiB–Ti composites is much lower than that for the monolithic TiB ceramic [32].

Fig. 6 also indicates that both the micro-hardness of the two phases in TiB–Ti composites and the micro-hardness difference between the two phases increase with rising sintering temperature. In SPS process, it is generally accepted that the number and the volume of the micro-pores in the composites decrease with increasing sintering temperature, thus the micro-hardness of the two phases in TiB–Ti composites increases. In addition, the needle-shaped TiB whiskers grow rapidly with rising sintering temperature, causing the volume fraction of the TiB phase in the indentation area increase rapidly. As a result, the micro-hardness difference between the two phases in the TiB–Ti composites increases.

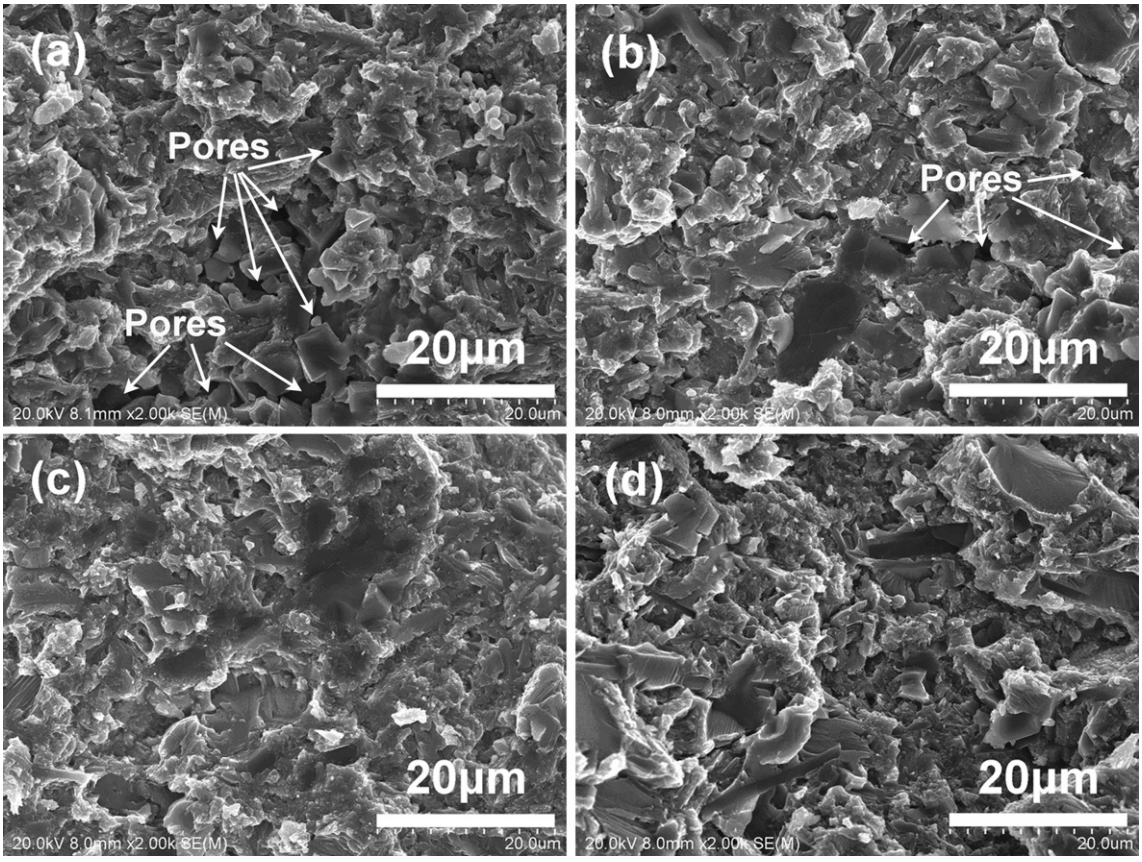

Fig. 4. Fracture surface of the TiB–Ti composites sintered at temperature: (a) 950 °C, (b) 1050 °C, (c) 1150 °C and (d) 1250 °C.

Fig. 8 shows the influence of sintering temperature on bending strength and fracture toughness of the TiB–Ti composites. Obviously, both the bending strength and the fracture toughness of the TiB–Ti composites increase with rising sintering temperatures. As the sintering temperature increase from 950 °C to 1250 °C, bending strength of the composites increase from 1012 MPa to 1160 MPa, and the fracture toughness increases from 7.8 MPa $m^{1/2}$ to 13.5 MPa $m^{1/2}$.

Both the grain size of the reinforcement and the relative density of the compacts have remarkable influence on bending strength of the metal–matrix composites. With rising sintering temperature, the relative density of the TiB–Ti composites synthesized by SPS process increases obviously, resulting in an increase in strength. However, TiB whiskers grow rapidly, leading to a decrease in bending strength due to the grain size effect. Finally, bending strength of the TiB–Ti composites increases slowly at the combined action of the two factors. Fracture toughness of the TiB–Ti composite increase with rising sintering temperature due to an increase in relative density. There is no doubt that the high fracture toughness of TiB–Ti composite sintered at 1250 °C by SPS process is mainly

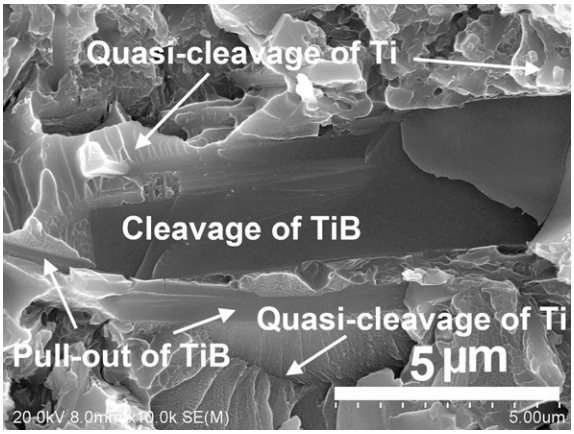

Fig. 5. Fracture surface of the TiB–Ti composite sintered at 1250 °C at high magnification.

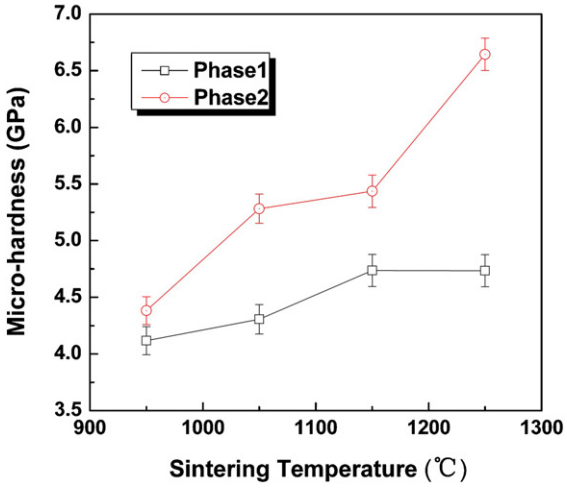

Fig. 6. Micro-hardness of the TiB–Ti composites sintered at different sintering temperatures.

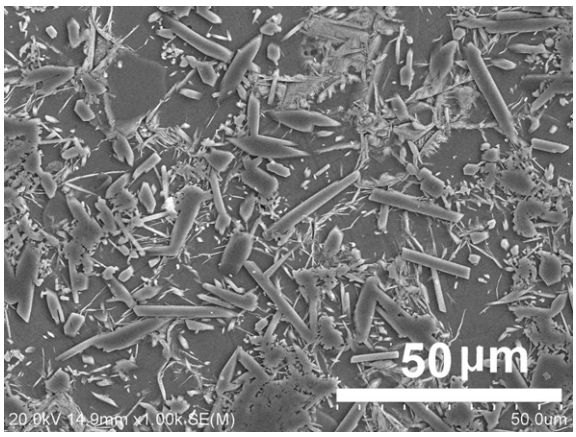

Fig. 7. SEM images of the TiB–Ti composite sintered at temperature of 1250 °C at low magnification, indicating the composite consist of two phases.

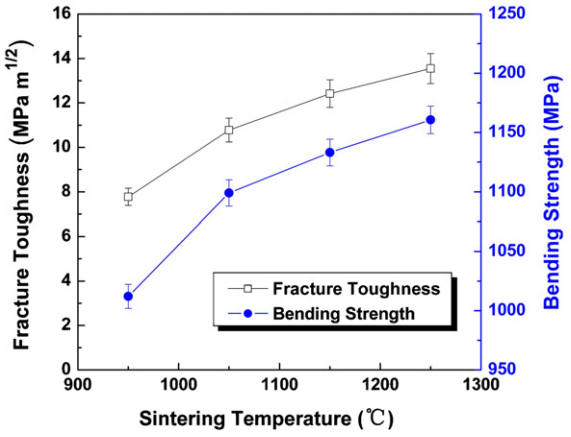

Fig. 8. Bending strength and fracture toughness of the TiB–Ti composites sintered at different temperatures.

resulted from the Ti matrix (about 74% in volume fraction). Moreover, the fine and needle-shaped TiB whiskers lead to much more grain boundaries, which can impede the propagation of cracks by the mechanism of crack deflection with absorbing much energy of micro-crack expansion. Additionally, pull-out and the micro-fracture of needle-shaped TiB whiskers on the fracture surface of the TiB–Ti composites also absorb much energy of micro-crack expansion. Thus, fracture toughness of the TiB–Ti metal–matrix composites synthesized by SPS process is improved remarkably.

4. Conclusions

The *in situ* synthesized TiB reinforced titanium matrix composites were synthesized by SPS process. The effect of sintering temperature on densification behavior and mechanical properties (micro-hardness, bending strength and fracture toughness) of the TiB–Ti composites were investigated. The results indicated that the TiB–Ti composite sintered at 1250 °C had the highest relative density of 99.6% along with bending strength of 1161 MPa and fracture toughness of 13.5 MPa $m^{1/2}$. In addition, with rising sintering temperature, the *in situ* synthesized TiB whiskers in the TiB–Ti metal–matrix composites prepared by SPS process grow rapidly, while the relative density of the composites increases obviously. Bending strength of the TiB–Ti composites increases slowly at the combined action of the two factors referred above. The fracture toughness of the composites is improved remarkably due to the large volume fraction of Ti matrix, the crack deflection, pull-out and the micro-fracture of the needle-shaped TiB grains.

Acknowledgements

The project was supported by Program for Peking Excellent Talents in the University under Grant No. 20061D0503200316, and the National Defense Pre-Research Foundation of China under Grant No. of 9140A12050209BQ0137.

References

[1] S. Birosca, J.Y. Buffiere, M. Karadge, M. Preuss, Acta Mater. 59 (2011) 1510–1522.
[2] T. Wang, H.Z. Guo, Y.W. Wang, X.N. Peng, Y. Zhao, Z.K. Yao, Mater. Sci. Eng. A 528 (2011) 2370–2379.
[3] F.C. Ma, P. Liu, W. Li, X.K. Liu, X.H. Chen, D. Zhang, Mater. Trans. 51 (2010) 1277–1280.
[4] H.B. Feng, Y. Zhou, D.C. Jia, Q.C. Meng, J.C. Rao, Cryst. Growth Des. 6 (2006) 1626–1630.
[5] S.C. Tjong, Y.W. Mai, Compos. Sci. Technol. 68 (2008) 583–601.
[6] R. Licheri, R. Orrù, G. Cao, Mater. Sci. Eng. A 367 (2004) 185–197.
[7] H.T. Tsang, C.G. Chao, Z.Y. Ma, Scripta Mater. 37 (1997) 1359–1365.
[8] L.L. Ye, Z.G. Liu, M.X. Quan, Z.Q. Hu, J. Appl. Phys. 80 (1996) 1910–1912.
[9] D. Ozyurek, T. Tuncay, Metallofiz. Nov. Tekh+. 32 (2010) 663–671.
[10] J.Q. Lu, J.N. Qin, W.J. Lu, Y. Liu, J.J. Gu, D. Zhang, J. Alloys Compd. 469 (2009) 116–122.
[11] B. Yang, E.L. Zhang, Y.X. Jin, Z.J. Zhu, S.Y. Zeng, J. Mater. Sci. Technol. 17 (2001) 103–104.
[12] S.S. Sahay, K.S. Ravichandran, R. Atri, J. Mater. Res. 14 (1999) 4214–4223.
[13] X.H. Zhang, Q. Xu, J.C. Han, V.L. Kvanin, Mater. Sci. Eng. A 348 (2003) 41–46.
[14] C. Poletti, G. Holtl, Kovove. Mater. 48 (2010) 87–95.
[15] S. Dubey, Y. Li, K. Reece, W.O. Soboyrjo, R.J. Lederich, Mater. Sci. Eng. A 266 (1999) 303–309.
[16] H.B. Feng, Q.C. Meng, Y. Zhou, D.C. Jia, Mater. Sci. Eng. A 397 (2005) 92–97.
[17] R. Licheri, R. Orrù, C. Musa, A.M. Locci, G. Cao, J. Alloys Compd. 478 (2009) 572–578.
[18] F.C. Wang, Z.H. Zhang, J. Luo, C.C. Huang, S.K. Lee, Compos. Sci. Technol. 69 (2009) 2682–2687.
[19] J.S. Kim, I.V. Povstugar, P.P. Choi, E.P. Yelsukov, Y.S. Kwon, J. Alloys Compd. 486 (2009) 511–514.
[20] Z.H. Zhang, F.C. Wang, L. Wang, S.K. Li, Mater. Lett. 62 (2008) 3987–3990.
[21] Z.H. Zhang, F.C. Wang, S.K. Li, M.W. Shen, S. Osamu, Mater. Charact. 59 (2008) 329–333.
[22] Z.H. Zhang, F.C. Wang, S.K. Li, L. Wang, Mater. Sci. Eng. A 527 (2010) 2099–2103.
[23] M. Kubota, P. Cizek, J. Alloys Compd. 457 (2008) 209–215.
[24] F. Monteverde, J. Alloys Compd. 428 (2007) 197–205.
[25] Z.H. Zhang, F.C. Wang, L. Wang, S.K. Lee, Mater. Sci. Eng. A 476 (2008) 201–205.
[26] G.S. Kim, D.H. Shin, Y.I. Seo, Y.D. Kim, Mater. Charact. 59 (2008) 1201–1205.
[27] Z.H. Zhang, X.B. Shen, F.C. Wang, S.K. Lee, L. Wang, Mater. Sci. Eng. A 527 (2010) 5947–5951.
[28] X.L. He, F. Ye, Z.Q. Zhou, H.J. Zhang, J. Alloys Compd. 496 (2010) 413–417.
[29] S.S. Sahay, K.S. Ravichandran, R. Arti, J. Mater. Res. 14 (1999) 4214–4223.
[30] Z.H. Zhang, X.B. Shen, S. Wen, J. Luo, S.K. Lee, F.C. Wang, J. Alloys Compd. 503 (2010) 145–150.
[31] W.J. Lu, D. Zhang, X.N. Zhang, R.J. Wu, T. Sakata, H. Mori, J. Alloys Compd. 327 (2001) 240–247.
[32] S. Nakane, Y. Takano, M. Yoshinaka, K. Hirota, O. Yamaguchi, J. Am. Ceram. Soc. 82 (1999) 1627–1628.